JACS
JOURNAL OF THE AMERICAN CHEMICAL SOCIETY
Article
pubs.acs.org/JACS

Mechanism of Inactivation of Neuronal Nitric Oxide Synthase by (*S*)-2-Amino-5-(2-(methylthio)acetimidamido)pentanoic Acid

Wei Tang,[†] Huiying Li,[‡] Emma H. Doud,[§] Yunqiu Chen,[§] Stephanie Choing,[†] Carla Plaza,[‡] Neil L. Kelleher,*[,§] Thomas L. Poulos,*[,‡] and Richard B. Silverman*[,†]

[†]Department of Chemistry, Department of Molecular Biosciences, Chemistry of Life Processes Institute, and Center for Molecular Innovation and Drug Discovery, Northwestern University, 2145 Sheridan Road, Evanston, Illinois 60208-3113, United States

[‡]Departments of Molecular Biology and Biochemistry, Chemistry, and Pharmaceutical Sciences, University of California, Irvine, California 92697-3900, United States

[§]Department of Chemistry, Department of Molecular Biosciences, Chemistry of Life Processes Institute, and Proteomics Center of Excellence, Northwestern University, 2145 Sheridan Road, Evanston, Illinois 60208-3113, United States

Supporting Information

ABSTRACT: Nitric oxide synthase (NOS) catalyzes the conversion of L-arginine to L-citrulline and the second messenger nitric oxide. Three mechanistic pathways are proposed for the inactivation of neuronal NOS (nNOS) by (*S*)-2-amino-5-(2-(methylthio)acetimidamido)pentanoic acid (**1**): sulfide oxidation, oxidative dethiolation, and oxidative demethylation. Four possible intermediates were synthesized. All compounds were assayed with nNOS, their IC_{50}, K_I, and k_{inact} values were obtained, and their crystal structures were determined. The identification and characterization of the products formed during inactivation provide evidence for the details of the inactivation mechanism. On the basis of these studies, the most probable mechanism for the inactivation of nNOS involves oxidative demethylation with the resulting thiol coordinating to the cofactor heme iron. Although nNOS is a heme-containing enzyme, this is the first example of a NOS that catalyzes an *S*-demethylation reaction; the novel mechanism of inactivation described here could be applied to the design of inactivators of other heme-dependent enzymes.

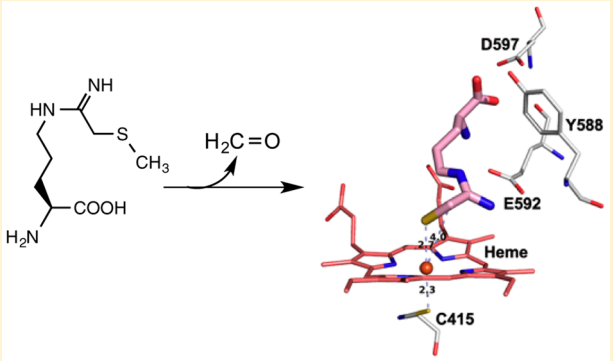

INTRODUCTION

Nitric oxide (NO) is an important cell-signaling molecule,[1,2] which is synthesized in vivo by nitric oxide synthase (NOS, EC 1.14.13.39).[3] In the presence of molecular oxygen, NOS converts L-arginine (L-Arg) to L-citrulline (L-Cit) and NO, with the reducing equivalents derived from oxidation of NADPH to $NADP^+$ (Scheme 1). During this two-step reaction, 2 and 1.5 equiv of O_2 and NADPH, respectively, are consumed to generate 1 equiv of NO.[4,5] There are three mammalian NOS isoforms: neuronal nitric oxide synthase (nNOS), important to neuronal signaling; inducible nitric oxide synthase (iNOS), which produces NO as a defense mechanism; and endothelial nitric oxide synthase (eNOS), which uses NO to regulate blood pressure. Low levels of NO are important as a second messenger and as a neurotransmitter.[6] However, NO can rapidly react with superoxide anion ($O_2\cdot^-$) to form peroxynitrite ($ONOO^-$).[7] The high levels of NO, $O_2\cdot^-$, and $ONOO^-$ are implicated in neurodegenerative diseases. The overproduction of NO in nNOS has been implicated in several pathological conditions; therefore, the inhibition of excess NO from nNOS has been an important approach for the design of drugs for the treatment of septic shock,[8] stroke,[9] migraine,[10] Alzheimer's,[11] Huntington's,[12] and Parkinson's,[13] diseases.[14−16] The NOS structure can be divided into three domains: a heme- and tetrahydrobiopterin-containing oxygenase domain and a FAD-, FMN-, and NADPH-containing reductase domain connected by a calcium−calmodulin domain.[17] Because of the essential roles of NO, nNOS inhibition to diminish excessive neuronal NO must be selective over iNOS and eNOS inhibition to prevent detrimental side effects.

To improve the binding selectivity of arginine mimetic inhibitors with nNOS, a sulfur atom was incorporated into a series of arginine amidines with the expectation that the sulfur atom might form a favorable interaction with the iron atom of the heme.[18] All but one of the sulfur-containing compounds prepared had poor selectivity and inhibitory activity. According to these earlier studies from our laboratory, compound **1** (Table S1, Supporting Information) is a selective, time-dependent irreversible inhibitor of nNOS, 185-fold more selective for nNOS inhibition than for eNOS inhibition, although only 3-fold more selective over iNOS. The crystal

Received: February 3, 2015
Published: April 15, 2015

DOI: 10.1021/jacs.5b01202
J. Am. Chem. Soc. 2015, 137, 5980−5989

Scheme 1. Synthesis of NO from L-Arginine

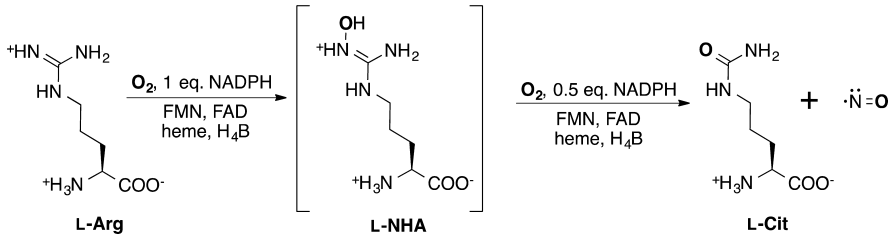

structure of **1** bound to the nNOS active site (Figure 1) shows that compound **1** is a type I ligand to the heme with its sulfur

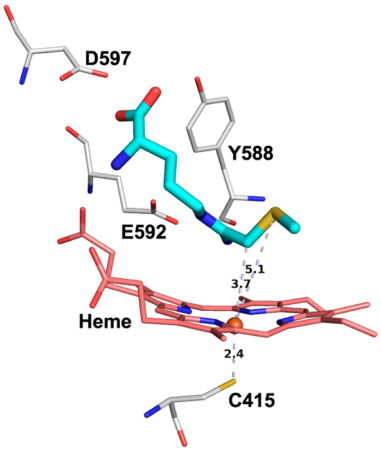

Figure 1. Crystal structure of **1** (cyan) bound in the active site of nNOS.[19] Key distances are marked in angstroms. All structure figures were prepared with PyMol (www.pymol.org).

atom and vicinal methylene carbon atom at a distance of 5.1 and 3.7 Å, respectively; on the basis of the reactivity of L-Arg and the inactivator N^5-(1-iminoethyl)-L-ornithine (L-NIO),[20] this predicted distance suggested that the sulfur atom could be oxidized by the heme as an initial step in an inactivation mechanism. Oxidation could result in the formation of **2** and/or **3**, thereby producing potential electrophiles having good leaving groups (methyl sulfenite or methyl sulfinite anions) and that could be attacked by an active site nucleophile (Figure 2, pathway A) or produce an enolate when an acidic proton between the amidine and sulfoxide or sulfone moieties is removed; enolate addition to a cofactor could lead to inactivation. Sulfide oxidation to the corresponding sulfoxide and sulfone metabolites is the most common heme-catalyzed reactions for sulfide-containing molecules.[21] Heme also can metabolize sulfides via oxidative dethiolation to the corresponding aldehyde products,[22] leading to metabolite **4** (Figure 2, pathway B), which might undergo Schiff base formation with a lysine residue. If **1** can be oxidized to **4** by nNOS, then **5**, which might arise from a hydroxide reaction with **2** or **3**, also could be oxidized to **4**. A third common metabolite reaction of sulfides is *S*-demethylation, which would convert **1** to **6** and formaldehyde; the generated thiol might form a complex with the heme iron atom (Figure 2, pathway C). All of these possible pathways are initiated by one-electron oxidation of the sulfide sulfur atom by a heme iron-oxo species, leading to the corresponding sulfenium cation radical (**7**, Figure 2).[23]

To test the viability of these proposed products and mechanisms, the inhibitory activity, inactivation kinetics,

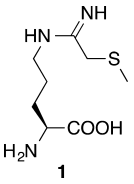

enzyme recovery after inactivation, metabolite formation, and modification of the heme by treatment of nNOS with **2**–**6** were determined. Other potential heme-coordinating sulfur-containing inhibitors of nNOS have been reported to be only inhibitors, not inactivators (**8**–**11**).[15,18] These inhibitors either have a longer linker length between the amidine moiety and the sulfur atom or a larger tail size attached to the sulfur atom. Our results support an inactivation mechanism that involves *S*-demethylation followed by heme–thiol complexation (Figure 2, pathway C).

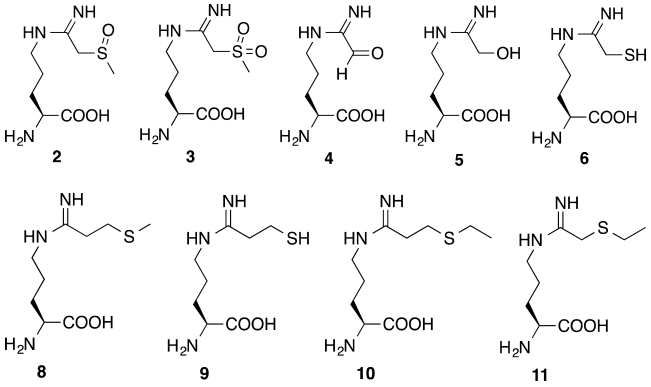

RESULTS AND DISCUSSION

Kinetics of Inhibition of nNOS by 1. Inhibition experiments were performed by measuring the velocity of NO generation after using different concentrations of the inhibitor and different concentrations of L-Arg (substrate). The NO hemoglobin assay was performed on **1**–**6** (see syntheses in the Supporting Information), and their IC_{50} and K_i values were obtained with rat nNOS (Table 1). Compound **6** was comparable in potency to **1**, compound **5** was half as potent, and the remainder displayed considerably weaker potency. Compounds **2** and **3** are possible metabolites from inactivation pathway A (Figure 2), but both were very weak inhibitors, and neither showed time-dependent inactivation with nNOS. The proposed metabolite in pathway B is **4**; **5** could be oxidized to **4**. Compounds **4** and **5** inhibited nNOS, but **4** is much less potent than **1**, and neither was a time-dependent inhibitor. Only **6** is more potent than **1** and also is a time- and concentration-dependent inactivator of nNOS; on the basis of steady-state kinetics, **6** appears to be a kinetically competent intermediate in the nNOS inactivation mechanism by **1**.

DOI: 10.1021/jacs.5b01202
J. Am. Chem. Soc. 2015, 137, 5980–5989

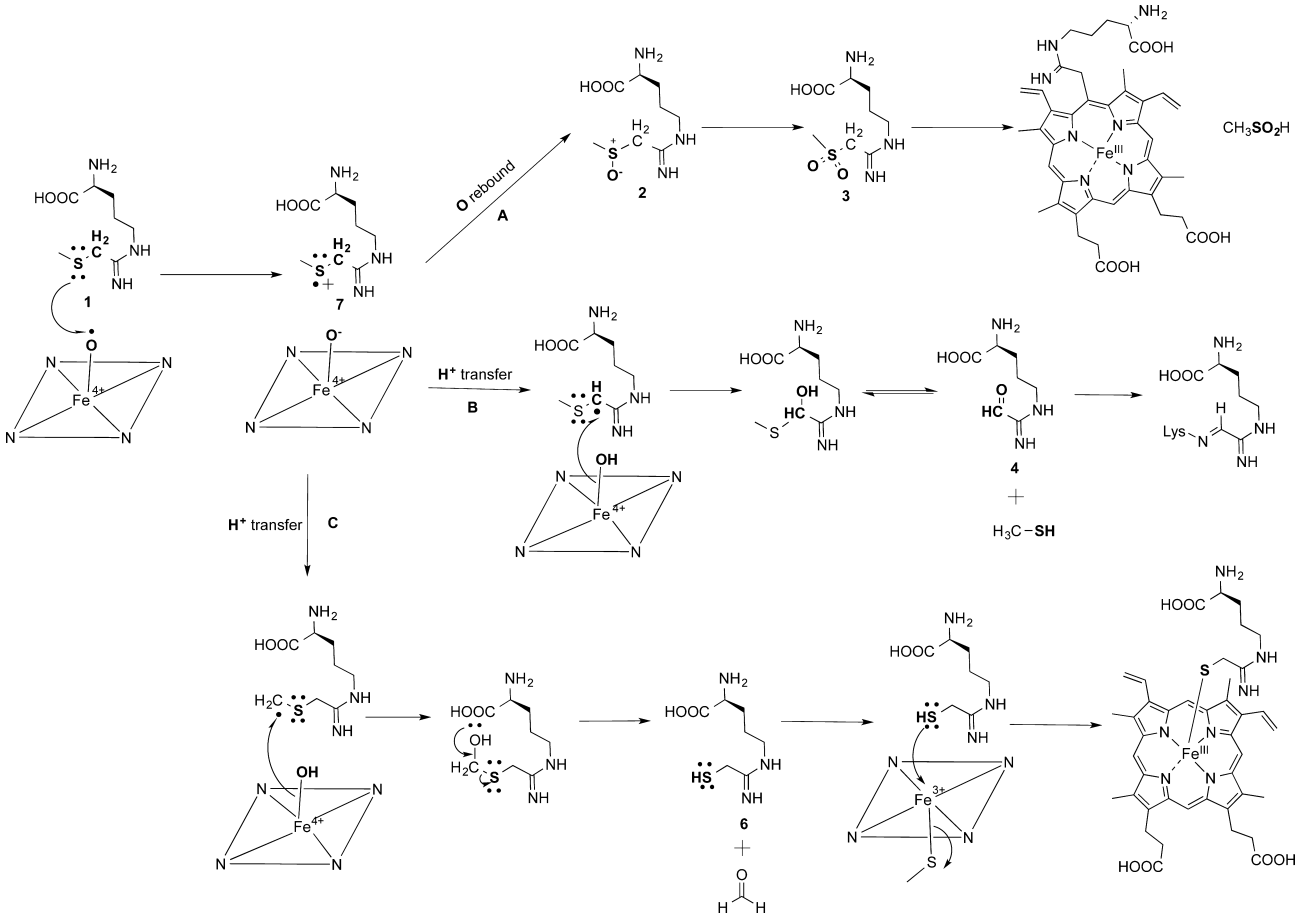

Figure 2. Three possible inactivation mechanisms for nNOS by **1**.

Table 1. IC_{50} and K_i Values for 1−6 with nNOS

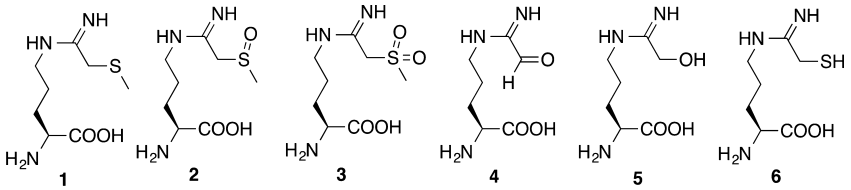

compound	IC_{50} (μM)	K_i (μM)
1	5.59 ± 0.55	0.64 ± 0.063
2	461 ± 20	53.0 ± 2.4
3	507 ± 49	58.3 ± 5.6
4	199 ± 7.1	22.9 ± 0.82
5	13.0 ± 0.67	1.50 ± 0.08
6	3.64 ± 0.15	0.42 ± 0.017

Experiments varying the concentrations of **1** and **6** with rat nNOS at room temperature were performed to determine their K_I and k_{inact} values (Figure 3). On the basis of their K_I values, **6** binds about 20 times more tightly to nNOS than does **1**, and the k_{inact} values show that **6** has about half the inactivation rate, indicating that **6** is about 9 times more efficient than **1** (Table 2), again indicating that, on the basis of steady-state kinetics, **6** is a kinetically competent intermediate. To support the hypothesized mechanism that generates **6** (Figure 2, pathway C), the nNOS generation of both **6** and formaldehyde was determined.

Identification of Amino Acid Metabolites during Inactivation of nNOS by 1. Liquid chromatography/mass spectrometry (LC/MS) was performed to detect possible metabolites from inactivation of nNOS by **1**. Incubation mixtures in replicate with neither inhibitor nor NADPH were studied as controls, and the data consistently showed that a small amount of **2** was generated after inactivation (Supporting Information, Figure S4). The mass of *o*-phthalaldehyde (OPA) and *β*-mercaptoethanol (BME)-derivatized **2** (compound **32**) had a LC retention time of 17.7 min, confirmed using a synthetic standard (Supporting Information, Figure S1). However, sulfur oxidation of **1** was found to occur during the LC/MS process. When this occurred, the *m*/*z* values of the oxidized compounds were observed at the same retention times as the standard nonoxidized compounds. For example, in both

DOI: 10.1021/jacs.5b01202
J. Am. Chem. Soc. 2015, 137, 5980−5989

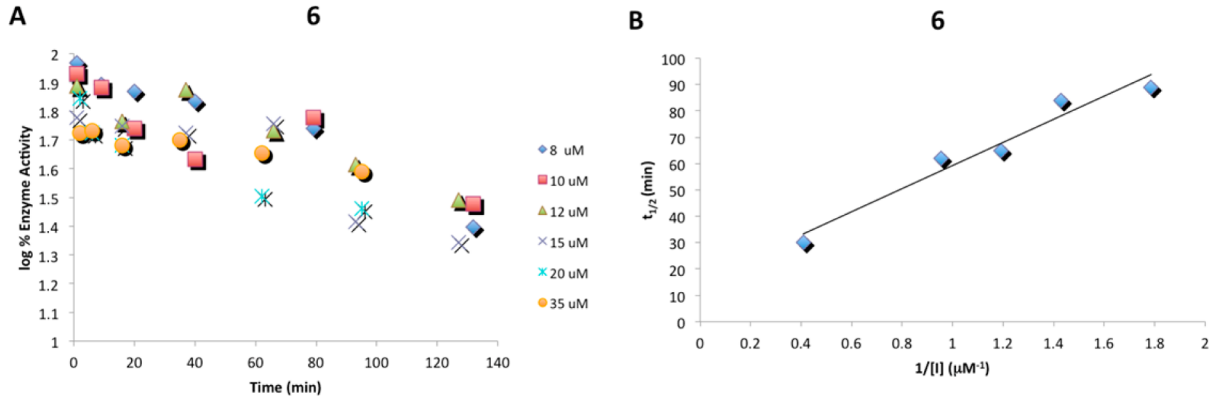

Figure 3. (A) Time- and concentration-dependent inactivation of nNOS by **6**. Each point represents the mean of three independent determinations. (B) Kitz–Wilson replot for the inactivation of nNOS by **6**; the equation for the plot is $y = 43.9x + 15.38$, $R^2 = 0.95$.

Table 2. K_I and k_{inact} Values (± Standard Error) for 1 and 6 with nNOS

	1	6
k_{inact} (min^{-1})	0.11 ± 0.01	0.046 ± 0.002
K_I (μM)	59.0 ± 6.0	2.9 ± 0.2
k_{inact}/K_I (μM^{-1} min^{-1})	0.0019 ± 0.0001	0.016 ± 0.001

the reaction and injection of standard **31**, an m/z corresponding to **32** appeared at the same retention time (t_R = 18.8 min, Figures 4 and Supporting Information, Figure S1). Whereas when a standard of **32** was injected, the m/z corresponding to both **32** and **33** appeared at t_R = 17.7 min, indicating the proclivity of the sulfur atom to oxidize under typical electrospray ionization conditions. The OPA and BME-derivatized **1** (Supporting Information, Figure S1) and **2** (Supporting Information, Figure S2) were used as standards. The data were confirmed by spiking with standards **31** and **32** (Supporting Information, Figure S3). This confirms that the more oxidized the compound (**33** > **32** > **31**), the earlier it elutes from reverse-phase high-performance liquid chromatography (HPLC), if it exists independently in the solution and is not created as an artifact of electrospray ionization (ESI) mass spectrometry.

It was further confirmed that **32** can be generated from the incubation of nNOS with **31**. No OPA and BME-derivatized **3**, **4**, or **6** were detected under these conditions. Compounds **4** and **6** were not detected using ESI in either the positive or negative mode, but **6** might undergo oxidative degradation.

The amount of **2** generated from the inactivation was determined using a standard linear curve (Supporting Information, Figure S4). Approximately 0.53 μM **2** is produced from the inactivation of nNOS by **1**, which converts to 2.9% turnover. Although **2** is a metabolite of this inactivation, its low concentration and poor inactivation rate constants indicate that it is not a kinetically competent intermediate.

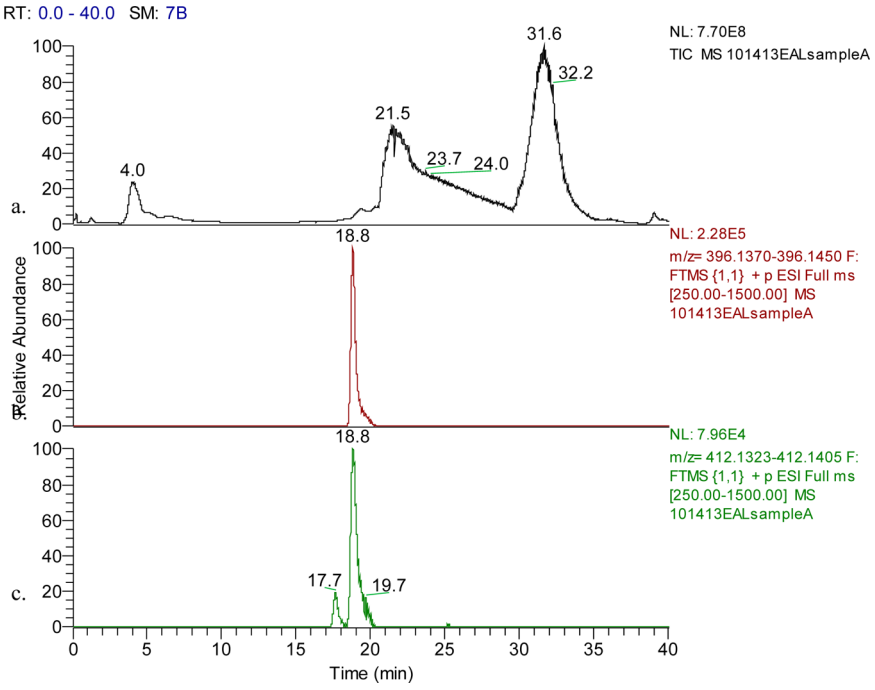

Figure 4. (a) Total ion chromatogram of LC/MS of inactivation of nNOS by **1**. (b) Extracted ion chromatogram of m/z corresponding to **31**. (c) Extracted ion chromatogram of m/z corresponding to **32**.

DOI: 10.1021/jacs.5b01202
J. Am. Chem. Soc. 2015, 137, 5980–5989

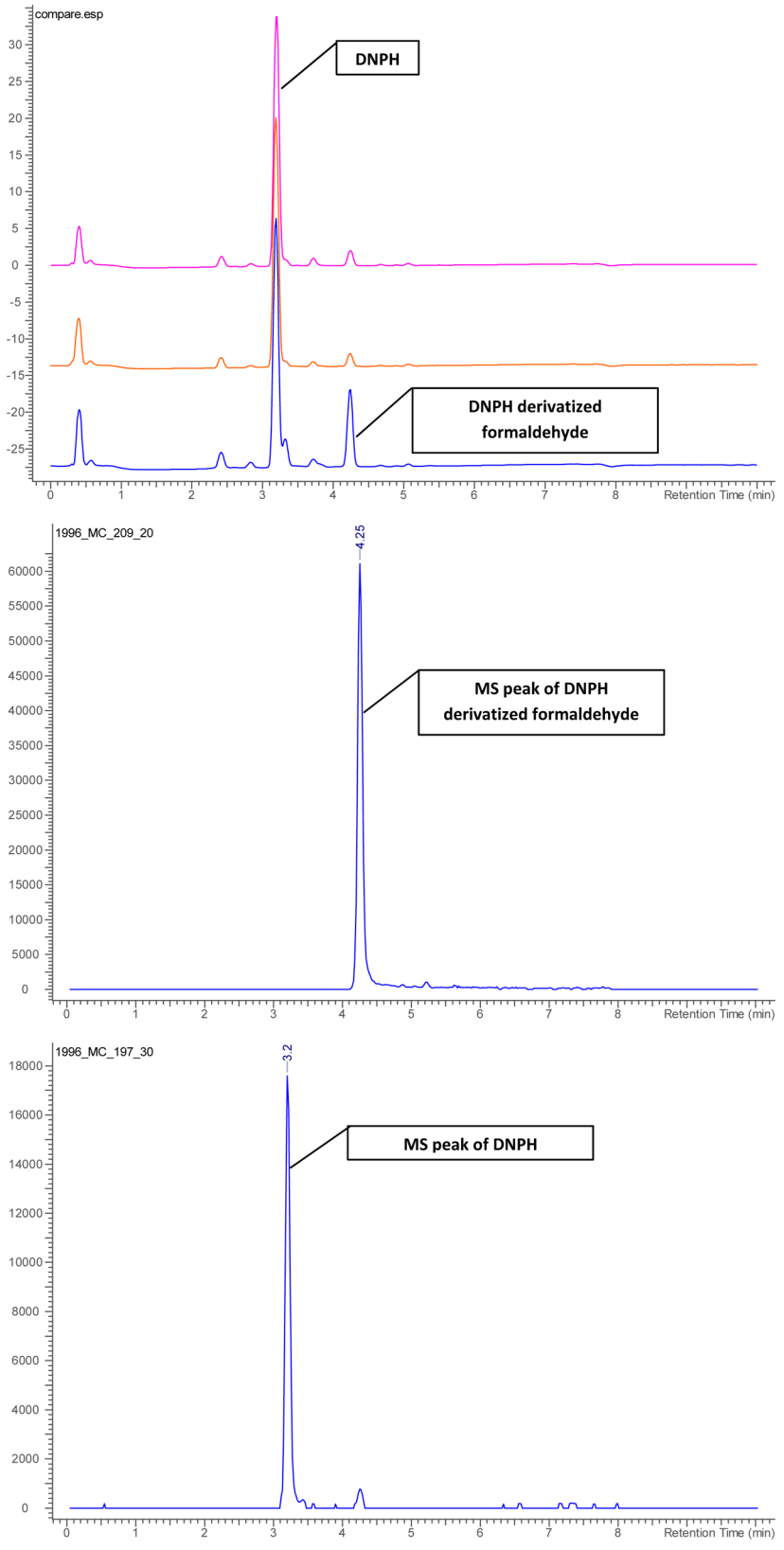

Figure 5. LC-MS of the NADPH-dependent formation of formaldehyde after inactivation of nNOS by **1**. Traces from top to bottom: LC/UV (360 nm) of control with no **1** (pink), LC/UV (360 nm) of control with no NADPH (orange), LC/UV (360 nm) of **1**-inactivated sample (blue); extracted ion chromatogram (LC/MS) of DNPH-derivatized formaldehyde; extracted ion chromatogram (LC/MS) of DNPH.

Identification of Formaldehyde as a Metabolite. Formaldehyde should be produced if **1** inactivates nNOS by mechanistic pathway C. The amount of formaldehyde was determined using 2,4-dinitrophenyl hydrazine (DNPH) derivatization. LC with both UV and MS detection was performed, and the generation of formaldehyde was identified (Figure 5).

DOI: 10.1021/jacs.5b01202
J. Am. Chem. Soc. 2015, 137, 5980−5989

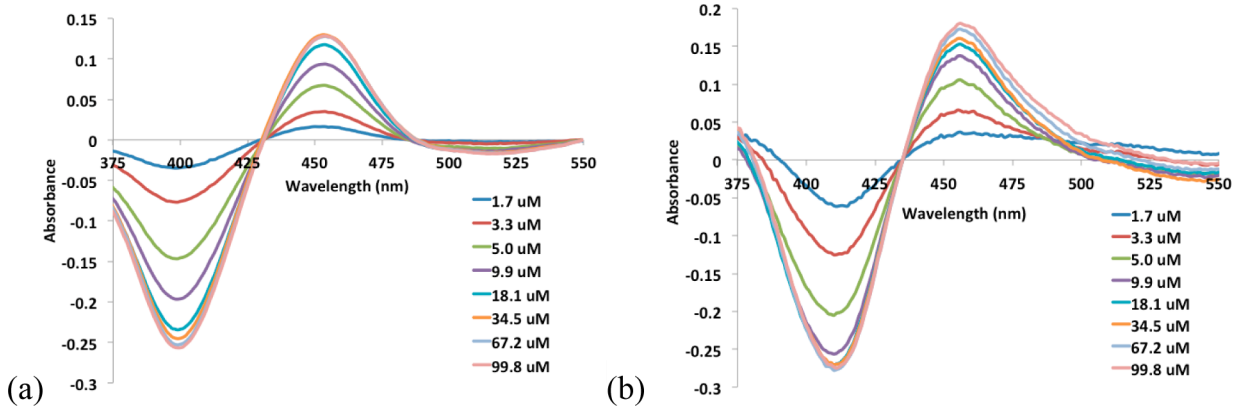

Figure 6. (a) Titration of rat nNOS−H_4B with **6**. (b) Titration of dithionite-reduced nNOS−H_4B with **6**. The plot was normalized at 430 and 435 nm, respectively. Note also, the trough positions are 400 and 410 nm in (a) and (b), respectively.

By using a standard curve for DNPH-derivatized formaldehyde (Supporting Information, Figure S5), there is about 38% conversion from **1**.

Ferric and Ferrous nNOS Difference Spectra with 6. For a heme thiolate enzyme such as NOS, the four heme pyrrole nitrogen atoms and the proximal heme ligand from a Cys residue form a pentacoordinated iron center. The NOS substrate L-Arg binds to the NOS active site through its extensive hydrogen-bonding interactions with the amino acid side chains lining the active site but without making ligation with heme. Therefore, the L-Arg is a type I, high-spin ligand generating a Soret peak at 395 nm typical of high-spin NOS and P450. However, if a heme type II, low-spin ligand is available at the distal side, such as imidazole or a water molecule, the heme becomes hexacoordinated, thereby showing a red shift of its Soret peak (427 nm for imidazole).[24] For NOS, the binding of the H_4B cofactor alone in the absence of L-Arg can still form a high-spin heme with a Soret peak at 400 nm; therefore, this can be used as the starting sample for titrations with a type II ligand.

Compound **6** was found to be a type II ligand as its binding to nNOS resulting in a bisthiolate species, having one native Fe−thiolate bond from the proximal Cys415 residue and a distal Fe−thiolate bond from **6**. Figure S6 (Supporting Information) shows the features of split Soret peaks characteristic of the bisthiolate. The apparent binding constant (K_s) of **6** can be determined from the difference spectra between a peak at 455 nm and a trough at 400 nm with rat nNOS, as shown in Figure 6a. This is in contrast to parent compound **1**, which is known to be a type I ligand from its difference spectra[18] and its crystal structure (Figure 1). We have also checked the binding of **6** to the dithionite-reduced nNOS−H_4B complex. The difference spectra exhibited a peak at 455 nm and a trough at 410 nm (Figure 6b). Again, **6** is still a type II ligand and may ligate to the ferrous heme iron as well. This provides support for pathway C as the inactivation mechanism. The apparent binding constants of **6**, K_s, to the ferric and ferrous nNOS are 1.8 ± 0.1 and 1.6 ± 0.3 μM, respectively; therefore, there is no significant difference.

Crystal Structures of 1−6. The crystal structures of **1** (Figure 1) as well as **2** and **3** (Figure 7) show a distance of about 5.1, 4.7, and 4.8 Å, respectively, between the S atom and the Fe atom. In addition, the lone-pair electrons of the sulfur atom on **1** are not properly oriented to interact with the iron−oxo bond required for S-oxidation in pathway A (Figure 2).

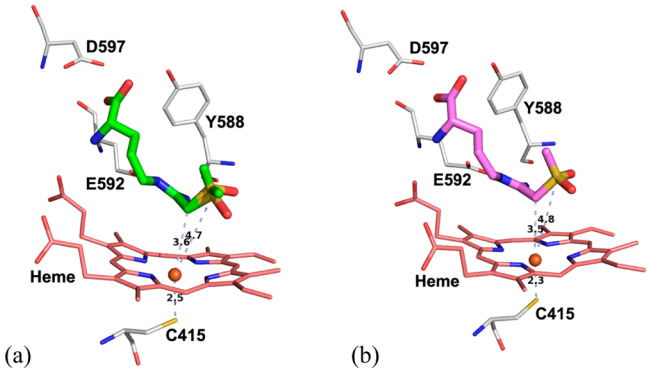

Figure 7. Crystal structures of **2** (a, green) and **3** (b, magenta) bound to the rat nNOS active site. Two alternate conformations were observed for the >S═O moiety of **2**, where the directions of methyl (green) and S═O (red) vary but the sulfur atom (yellow) remains in the same position. Key distances are marked in angstroms.

Although once the heme iron is reduced and molecular oxygen is bound, the ligand conformation might undergo some changes that are not reflected in the crystal structures, S-oxidation is not likely the major turnover pathway considering the far Fe−S distance observed in the structures. On the other hand, S-demethylation of **1** to give **6** should be easier than S-oxidation, since the S−C bond is more accessible to the heme−oxo species, leading to pathway C for nNOS inactivation (Figure 2).

The distance between the vicinal methylene carbon atom and the heme iron is 3.7 Å in **1** (Figure 1), which is a reasonable distance for carbon oxidation, and potential intermediate **4** might be generated after oxidation. The crystal structure for **4** bound to the nNOS active site (Figure 8a) shows a binding mode similar to that of **1** (Figure 1). A crystal structure was also obtained for **5** bound to the nNOS active site (Figure 8b). Its binding mode is similar to that of the substrate N^{ω}-hydroxyarginine. The main difference between **4** and **5** is that the C═O group in **4** bends significantly away from the plane defined by the N_e, C_z, C_h, and N_h atoms, while in **5** the hydroxyl group is almost coplanar. As a result, binding of **5** to nNOS is stronger than **4** (Table 1) because of an extra H bond from the OH to the backbone amide of Gly586, while the C═O group in **4** makes no significant contact with protein.

Although the difference spectra indicated that **6** was a type II ligand (Figure 6), the Fe−S bond was not observed initially in the crystal structures for **6** bound to the nNOS active site. While the first structure obtained at pH 6.0 (pH of the

DOI: 10.1021/jacs.5b01202
J. Am. Chem. Soc. 2015, 137, 5980−5989

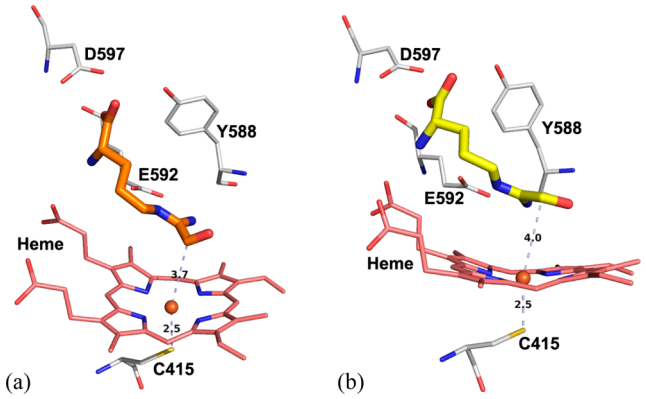

Figure 8. Crystal structures of **4** (a, orange) or **5** (b, yellow) bound to the rat nNOS active site. Key distances are marked in angstroms.

crystallization buffer) showed a type I ligand binding mode for **6** with its S atom pointing away from the heme (data not shown), the second structure obtained by transferring crystals to the cryo-soaking solutions at pH 7.5 revealed two alternate conformations (Figure 9a). The major conformation (70%) still

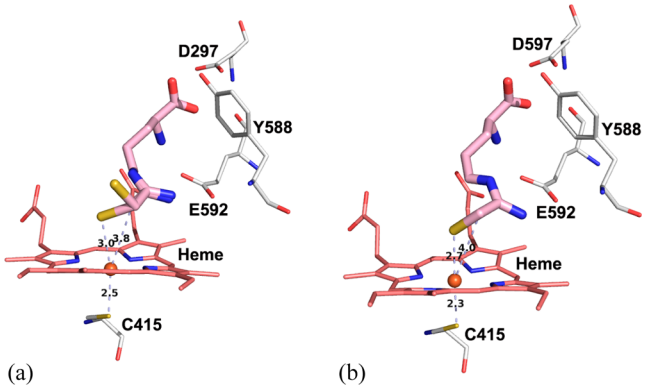

Figure 9. (a) Crystal structure of **6** (pink) bound to the rat nNOS active site obtained at pH 7.5; two alternate conformations were found for the terminal sulfur atom. (b) The ferric nNOS–**6** structure obtained with the composite data collection procedure at pH 7.5; a ligation bond at 2.7 Å was observed.

had the S atom pointing away from the heme, similar to what was seen at pH 6.0; the other conformation (30%) showed the S atom pointing toward the heme with an Fe–S distance of 3.0 Å. The observed Fe–S distance is longer than that for an Fe–S ligation bond, but reduction of the heme iron in the X-ray beam very likely alters ligand affinity.

In previous work,[18] we developed a composite data collection protocol that ensures the iron remains in the ferric oxidation state. This involves merging data obtained from several crystals, each of which is exposed to X-rays for only a short time, thereby avoiding iron reduction. The structure of **6** bound to nNOS obtained using this approach shows a single conformation of **6** with its S atom 2.7 Å from the heme iron (Figure 9b). Although this is longer than the proximal Fe–thiolate bond length with the Cys ligand, it is reasonable for a ligation bond in an iron bisthiolate species (there is no known bisthiolate heme in native proteins). This observed ligation bond provides the structural basis for pathway C (Figure 2) as the inactivation mechanism.

CONCLUSIONS

Compound **1** is an inactivator of nNOS; three possible mechanistic pathways were proposed. The corresponding metabolites were synthesized, and their enzymatic kinetic data were determined. Compounds **2**, **3**, and **4** showed much larger IC_{50} values than **1**, suggesting that they are not relevant to the inactivation mechanism. Compound **6** gave a slightly smaller K_i value compared to **1**, indicating that they have comparable binding energies. Furthermore, **6** turns over about 10 times faster than **1** with nNOS, which suggests, on the basis of steady-state kinetics, that **6** is a kinetically competent intermediate for inactivation of nNOS by **1**. The production of formaldehyde occurred in 38% of **1** turnovers to products, although LC/MS did not reveal the presence of **6** after inactivation. The generation of **2** in about 3% of turnovers was confirmed, but this could be an irrelevant side reaction. The crystal structure of **6** bound to nNOS confirmed the existence of an Fe–S bond. These experiments support an inactivation mechanism that involves heme oxo S-demethylation and coordination of the thiolate produced with the heme iron (Figure 2, pathway C). Although nNOS is a heme-containing enzyme, this is the first example of an *S*-demethylation reaction catalyzed by nNOS, and it also is a novel inactivation mechanism, which could be applied to other heme-dependent enzymes.

EXPERIMENTAL SECTION

General Methods. All chemicals were purchased from Sigma–Aldrich and were used without further purification. LC/MS studies of amino acids were carried out on an Agilent 1200 LC and a Thermo Exactive (ESI) mass spectrometer using a Phenomenex (Torrance, CA, USA) Luna C18 100A (5 μm, 150 cm × 2 cm) column. Determination of formaldehyde and analytical reverse-phase HPLC/MS were performed on an Agilent 1200 series system (Agilent Technologies, Santa Clara, CA, USA) using a Phenomenex Gemini-NX C18 column (4.6 cm × 50 cm, 5 μm). This system was equipped with an Agilent G1315C DAD detector and an Agilent 6130 quadrupole MS detector. Preparative runs were performed with a Phenomenex Gemini-NX C18 column (21.20 cm × 150 cm, 5 μm).

Chemical Syntheses. See details in the Supporting Information.

*(S)-2-Amino-5-(2-(methylthio)acetimidamido)pentanoic Acid (**1**).* This compound was prepared according to the method of Litzinger et al.[18]

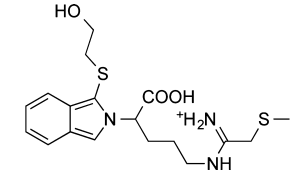

Chemical Formula: $C_{18}H_{26}N_3O_3S_2^+$
Exact Mass: 396.1410
31

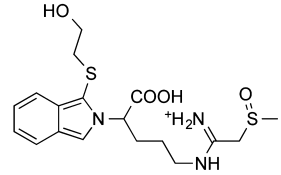

Chemical Formula: $C_{18}H_{26}N_3O_4S_2^+$
Exact Mass: 412.1359
32

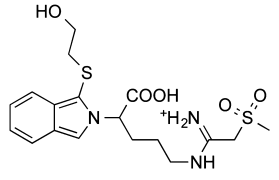

Chemical Formula: $C_{18}H_{26}N_3O_5S_2^+$
Exact Mass: 428.1308
33

*(2S)-2-Amino-5-(2-(methylsulfinyl)acetimidamido)pentanoic Acid (**2**).* This compound was prepared from 1 equiv oxidation of **1** with H_2O_2.

DOI: 10.1021/jacs.5b01202
J. Am. Chem. Soc. 2015, 137, 5980–5989

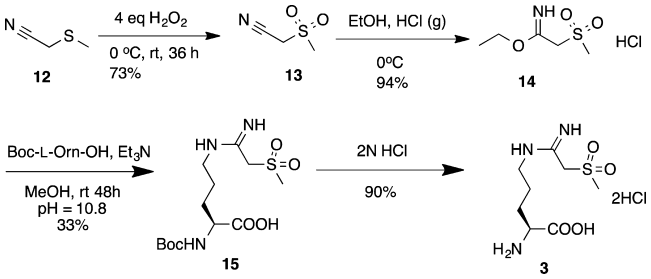

*(S)-2-Amino-5-(2-(methylsulfonyl)acetimidamido)pentanoic Acid (**3**).* This compound was prepared following the synthetic route above.

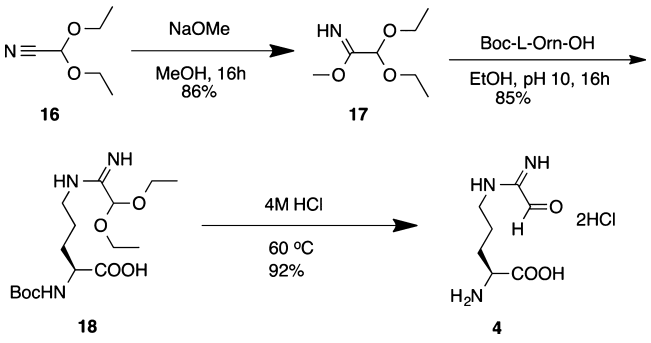

*(S)-2-Amino-5-(2-oxoacetimidamido)pentanoic Acid (**4**).* This compound was prepared following the synthetic route above.

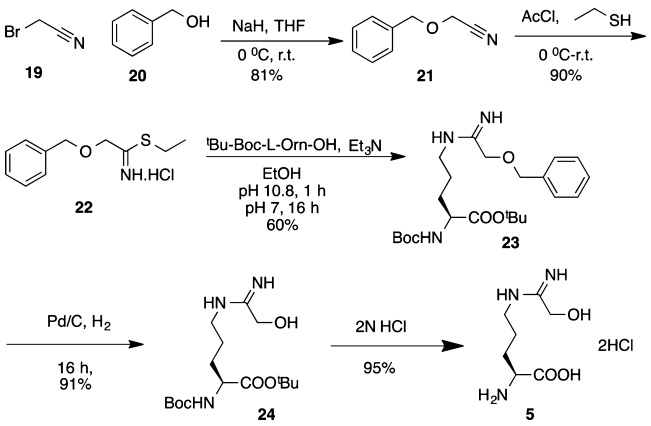

*(S)-2-Amino-5-(2-hydroxyacetimidamido)pentanoic Acid (**5**).* This compound was prepared following the synthetic route above.[25]

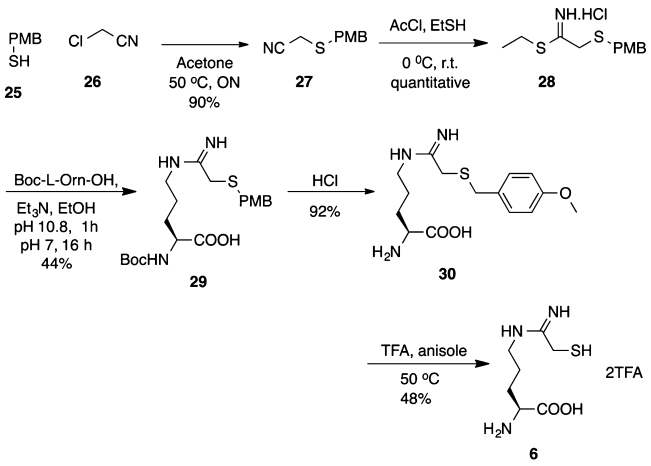

*(S)-2-Amino-5-(2-mercaptoacetimidamido)pentanoic Acid (**6**).* This compound was prepared following the synthetic route above.[26,27]

Hemoglobin NO Generation Assay. Recombinant rat nNOS was expressed and purified from *Escherichia coli*.[28] The production of NO was measured by the rapid oxidation of oxyHb to metHb by NO.[29] The inhibition assays contained 10 μM L-Arg, 104 μM NADPH, 833 μM $CaCl_2$, 3 U CaM, 80 μM H_4B, 0.75 μg of oxyHb, and different amounts of inhibitors. The final volume was adjusted to 600 μL with 100 mM HEPES buffer, pH 7.4. The enzymatic reaction was initiated by addition of 10 μL of nNOS stock, and the rate of NO production was monitored by the change in absorbance at 401 nm in the initial 60 s on a spectrophotometer at 37 °C. For K_i determinations, IC_{50} values were calculated using nonlinear regressions (dose−response inhibition, four-parameter variable slope). Subsequent K_i values were calculated using the Cheng−Prusoff relationship: $K_i = IC_{50}/(1 + [S]/K_m)$ (K_m for murine nNOS is 6.9 μM).[30]

LC/MS Study of 1. The inactivation mixture of **1** with nNOS was derivatized with OPA and BME. Inactivation mixtures contained 56 μM **1**, 0.0055 mg of catalase, 6% glycerol, 3.51 mM NADPH, 0.56 mM H_4B, 3 mM $CaCl_2$, 0.018 U CaM, and 12 μM nNOS stock in a total volume of 100 μL. HEPES buffer (100 mM, pH 7.4) was used as the solvent. The mixture was incubated at 37 °C for 3 h until completion of inactivation. Aliquots (10 μL) were removed and added to 20 μL of OPA/BME (20:1, v/v) reagent. The sample was injected into the HPLC chromatograph; the gradient was started with 2% B, held for 5 min, and then, 2−98% B over 30 min (A = H_2O with 0.1% formic acid and B = MeCN with 0.1% formic acid), followed by a wash of 98% B for another 5 min. MS data were collected in positive ESI mode.

Irreversible Inhibition Kinetics. The same inactivation mixtures were prepared as above. The reactions were initiated by the addition of enzyme, and 10 μL aliquots were removed at specified time points and tested via the initial velocity assay. Controls were performed by replacing the inhibitor or NADPH with HEPES buffer. K_I and k_{inact} values were determined by the method of Kitz and Wilson.[31]

DNPH Derivatization of Formaldehyde. DNPH-derivatization reactions were prepared by mixing 20 μL of formaldehyde standard or sample with 10 μL of 20 mM DNPH in 0.4 M H_2SO_4 in 10% H_2O, 90% MeCN. The derivatization reactions were complete in 10 min. The sample was injected onto a Phenomenex Gemini-NX C18 column at 360 nm; mobile phase A is H_2O with 1% formic acid, and B is MeCN with 1% formic acid. A gradient from 10−90% B was run over 7 min at 1.0 mL/min. Then, B was increased to 100% in 0.1 min and held until 10 min. Under these conditions, DNPH eluted at 3.2 min, and DNPH-formaldehyde eluted at 4.3 min. A DNPH−formaldehyde standard curve (R^2 = 0.981) was linear from 10 to 120 μM.

Spectral Titration of Ferrous and Ferric nNOS with 6. These experiments were similar to those reported earlier.[18] The inhibitor−ferric difference spectrometry assays were performed on a Cary 300 (Agilent) spectrophotometer. Full-length nNOS (5 μM) in 600 μL of HEPES buffer (50 mM, pH 7.5, 100 mM NaCl) was titrated with 1 or 2 μL of **6**, and spectral changes were monitored from 350 to 550 nm. The total volume of the aliquots did not exceed 2% of the buffer volume.

For ferrous difference spectrometry assays, the spectral titrations of inhibitor **6** binding to the ferrous nNOS were carried out under anaerobic conditions with a Cary 4 (Varian) spectrophotometer. The HEPES buffer (50 mM, pH 7.5, 100 mM NaCl) was sealed in serum vials and degassed by purging the solution with ultrapure argon and pulling vacuum in the head space of the vial for a few alternating cycles within 2 h. All of the inhibitor stock solutions were made with degassed buffer inside a glovebox (COY Laboratory Products, Inc.). The full-length nNOS was reduced by adding grains of dithionite, and then, the reduced sample was passed through a 10-DG desalting column (Bio-Rad Laboratories) in the glovebox to remove excess dithionite. An aliquot of reduced nNOS was used to take a spectral scan, which showed a Soret peak at 410 nm, confirming the reduction of heme. To both the sample and reference septum-sealed cuvettes was added 600 μL of buffer containing ~6.2 μM nNOS; then, the baseline was set up with both cuvettes in place using the double beam mode of the instrument. Each addition of 1−2 μL of **6** to the sample cuvette, with stock concentrations of 1, 5, and 20 mM, was performed inside the glovebox. The total volume of the aliquots was less than 2%

DOI: 10.1021/jacs.5b01202
J. Am. Chem. Soc. 2015, 137, 5980−5989

of the buffer volume (600 μL) in the sample cuvette. After each addition, spectral scans were carried out in the range 350−600 nm and repeated a few times until no further spectral change was observed.

The absorbance differences from the peak (~455 nm) to the trough (400 nm for ferric and 410 nm for ferrous heme) positions were extracted from titration curves and then plotted against the micromolar concentration of inhibitor **6**. The resulting plots showing the saturation features that could not be fit properly with a hyperbolic function in SigmaPlot ($\Delta A = B_{max}[L]/(K_s + [L])$; instead, a quadratic function was used to derive the apparent K_s values from the plot:

$$\Delta A = A_0 + (B_{max}/2[E])((K_s + [E] + [L]) - ((K_s + [E] + [L])^2 - 4[E][L])^{1/2})$$

where B_{max} is the maximum absorbance change to infinite ligand concentration, [E] is the total enzyme concentration, [L] is the ligand concentration, and A_0 is a constant.

Inhibitor Complex Crystal Preparation. The nNOS heme domain proteins used for crystallographic studies were produced by limited trypsin digest from the corresponding full-length enzymes and further purified through a Superdex 200 gel filtration column (GE Healthcare); the nNOS heme domain (at 9 mg/mL containing 20 mM histidine) was used for the sitting drop vapor diffusion crystallization setup under conditions as described previously.[32] Fresh crystals (1−2 days old) were first passed stepwise through cryoprotectant solutions and then soaked with 10 mM inhibitor for 4−6 h at 4 °C before being flash cooled with liquid nitrogen.

X-ray Diffraction Data Collection, Data Processing, and Structural Refinement. The cryogenic (100 K) X-ray diffraction data were collected remotely at the Stanford Synchrotron Radiation Lightsource or Advanced Light Source (ALS) through the data collection control software Blu-Ice[33] and a crystal mounting robot. When a Q315r CCD detector was used, 90−100° of data were typically collected with 0.5° per frame. If a Pilatus pixel array detector was used, 140−150° of fine-sliced data were collected with 0.2° per frame. Raw CCD data frames were indexed, integrated, and scaled using HKL2000,[34] but the pixel array data were processed with XDS[35] and scaled with Scala (Aimless).[36] The composite data of nNOS bound with **6** were collected with about 20 crystals at ALS BL12.3.1. For each crystal, a snapshot was taken, and the image was indexed to get the orientation matrix. The Strategy routine in MOSFLM[37] was used to determine the starting scanning angle for data collection. Then 5° of data at 1 s exposure per frame (1°) were collected. Once the next crystal was mounted and the snapshot image was indexed, the Strategy in MOSFLM was used again to determine the best starting angle for the current crystal by incorporating crystal orientation matrices from the previous crystal(s). The calculation was necessary to avoid collecting data in the reciprical space that had been covered by the data from the previous crystals. Data frames from multiple crystals were integrated with XDS and then merged and scales with Aimless. Data frames from certain crystals which showed poor merging *R* values were rejected in the final scaling.

The binding of inhibitors was detected by the initial difference Fourier maps calculated with REFMAC.[38] The inhibitor molecules were then modeled in COOT[39] and refined using REFMAC or PHENIX.[40] Water molecules were added in REFMAC or PHENIX and checked by COOT. The TLS[41] protocol was implemented in the final stage of refinements with each subunit as one TLS group. The omit Fo − Fc density maps were calculated by repeating the last round of TLS refinement with the inhibitor coordinate removed from the input PDB file to generate the map coefficients DELFWT and SIGDELWT. The refined structures were validated in COOT before deposition in the protein data bank. The crystallographic data collection and structure refinement statistics are summarized in Table S2 (Supporting Information) with the PDB accession codes included.

■ ASSOCIATED CONTENT

Supporting Information

Structures of compounds **1**−**6** and **31**−**33**; HPLC of metabolites of nNOS oxidation of **1**; LC/MS of formaldehyde formation from inactivation of nNOS by **1**; crystallographic data; chemical synthesis; and NMR spectra of final products. The Supporting Information is available free of charge on the ACS Publications website at DOI: 10.1021/jacs.5b01202.

■ AUTHOR INFORMATION

Corresponding Authors

*n-kelleher@northwestern.edu
*poulos@uci.edu
*Agman@chem.northwestern.edu

Notes

The authors declare no competing financial interest.

■ ACKNOWLEDGMENTS

This work was supported by the National Institutes of Health (GM049725 to R.B.S. and GM057353 to T.L.P.).

■ REFERENCES

(1) Moncada, S.; Palmer, R. M.; Higgs, E. A. *Biochem. Pharmacol.* **1989**, *38*, 1709−1715.
(2) Marletta, M. A. *Trends Biochem. Sci.* **1989**, *14*, 488−492.
(3) Kerwin, J. F.; Heller, M. *Med. Res. Rev.* **1994**, *14*, 23−74.
(4) Stuehr, D. J.; Griffith, O. W. *Adv. Enzymol. Relat. Areas Mol. Biol.* **1992**, *65*, 287−346.
(5) Marletta, M. A. *Adv. Exp. Med. Biol.* **1993**, *338*, 281−284.
(6) Moncada, S.; Palmer, R. M. J.; Higgs, E. A. *Pharmacol Rev.* **1991**, *43*, 109−142.
(7) Naseem, K. M. *Mol. Aspects Med.* **2005**, *26*, 33−65.
(8) Comini, L.; Boraso, A.; Bachetti, T.; Bernocchi, P.; Pasini, E.; Bastianon, D.; Curello, S.; Terracciano, C. M.; Ceconi, C.; Ferrari, R. *Pharmacol. Res.* **2005**, *51*, 409−417.
(9) Li, H.; Forstermann, U. *J. Pathol.* **2000**, *190*, 244−254.
(10) Ramachandran, R.; Ploug, K. B.; Hay-Schmidt, A.; Olesen, J.; Jansen-Olesen, I.; Gupta, S. *Neurosci. Lett.* **2010**, *484*, 192−196.
(11) Dorheim, M. A.; Tracey, W. R.; Pollock, J. S.; Grammas, P. *Biochem. Biophys. Res. Commun.* **1994**, *205*, 659−665.
(12) Norris, P. J.; Waldvogel, H. J.; Faull, R. L.; Love, D. R.; Emson, P. C. *Neuroscience* **1996**, *72*, 1037−1047.
(13) Giasson, B. I.; Duda, J. E.; Murray, I. V.; Chen, Q.; Souza, J. M.; Hurtig, H. I.; Ischiropoulos, H.; Trojanowski, J. Q.; Lee, V. M. *Science.* **2000**, *290*, 985−989.
(14) Nakamura, T.; Lipton, S. A. *Antioxid. Redox Signaling* **2008**, *10*, 87−101.
(15) Dawson, V. L.; Dawson, T. M. *Prog. Brain Res.* **1998**, *118*, 215−229.
(16) Vallance, P. P.; Leiper, J. J. *Nat. Rev. Drug Discovery* **2002**, *1*, 939−950.
(17) Ghosh, D. K.; Abu-Soud, H. M.; Stuehr, D. J. *Biochemistry* **1995**, *34*, 11316−11320.
(18) Litzinger, E. A.; Martasek, P.; Roman, L. J.; Silverman, R. B. *Bioorg. Med. Chem.* **2006**, *14*, 3185−3198.
(19) Martell, J. D.; Li, H.; Doukov, T.; Martásek, P.; Roman, L. J.; Soltis, M.; Poulos, T. L.; Silverman, R. B. *J. Am. Chem. Soc.* **2010**, *132*, 798−806.
(20) Zhu, Y.; Nikolic, D.; Silverman, R. B. *J. Am. Chem. Soc.* **2005**, *127*, 858−868.
(21) Mitchell, S. C.; Waring, R. H. *Drug Metab. Rev.* **1986**, *16*, 255−284.
(22) Oae, S.; Mikami, A.; Matsuura, T.; Ogawa-Asada, K.; Watanabe, Y.; Fujimori, K.; Iyanagi, T. *Biochem. Biophys. Res. Commun.* **1985**, *131*, 567−573.

DOI: 10.1021/jacs.5b01202
J. Am. Chem. Soc. 2015, 137, 5980−5989

(23) Goto, Y.; Matsui, T.; Ozaki, S.-i.; Watanabe, Y.; Fukuzumi, S. *J. Am. Chem. Soc.* **1999**, *121*, 9497−9502.
(24) McMillan, K.; Masters, B. S. S. *Biochemistry* **1993**, *32*, 9875−9880.
(25) Meyers, A. I.; Oppenlaender, T. *J. Am. Chem. Soc.* **1986**, *108*, 1989−1996.
(26) Fang, X.; Li, J.; Wang, C. *Org. Lett.* **2013**, *15*, 3448−3451.
(27) Tsui, G. C.; Glenadel, Q.; Lau, C.; Lautens, M. *Org. Lett.* **2011**, *13*, 208−211.
(28) Roman, L. J.; Sheta, E. A.; Martásek, P.; Gross, S. S.; Sessa, W. C.; Masters, B. S. S. *Proc. Natl. Acad. Sci. U.S.A.* **1995**, *92*, 8428−8432.
(29) Hevel, J. M.; Marletta, M. A. *Methods Enzymol.* **1994**, *233*, 250−258.
(30) Cheng, Y.-C.; Prusoff, W. H. *Biochem. Pharmacol.* **1973**, *22*, 3099−3108.
(31) Kitz, R.; Wilson, I. B. *J. Biol. Chem.* **1962**, *237*, 3245−3249.
(32) Li, H.; Shimizu, H.; Flinspach, M.; Jamal, J.; Yang, W.; Xian, M.; Cai, T.; Wen, E. Z.; Jia, Q.; Wang, P. G.; Poulos, T. L. *Biochemistry.* **2002**, *41*, 13868−13875.
(33) McPhillips, T. M.; McPhillips, S. E.; Chiu, H. J.; Cohen, A. E.; Deacon, A. M.; Ellis, P. J.; Garman, E.; Gonzalez, A.; Sauter, N. K.; Phizackerley, R. P.; Soltis, S. M.; Kuhn, P. *J. Synchrotron Radiat.* **2002**, *9*, 401−406.
(34) Otwinowski, Z.; Minor, W. *Methods Enzymol.* **1997**, *276*, 307−326.
(35) Kabsch, W. *Acta Crystallogr.* **2010**, *D66*, 125−132.
(36) Evans, P. R. *Acta Crystallogr.* **2006**, *D62*, 72−82.
(37) Leslie, A. G. W. *Jnt CCP4/ESF-EACMB Newsl. Protein Crystallogr.* **1992**, *26*, 27−33.
(38) Murshudov, G. N.; Vagin, A. A.; Dodson, E. J. *Acta Crystallogr.* **1997**, *D53*, 240−255.
(39) Emsley, P.; Cowtan, K. *Acta Crystallogr.* **2004**, *D60*, 2126−2132.
(40) Adams, P. D.; Afonine, P. V.; Bunkóczi, G.; Chen, V. B.; Davis, I. W.; Echols, N.; Headd, J. J.; Hung, L.-W.; Kapral, G. J.; Grosse-Kunstleve, R. W.; McCoy, A. J.; Moriarty, N. W.; Oeffner, R.; Read, R. J.; Richardson, D. C.; Richardson, J. S.; Terwilliger, T. C.; Zwart, P. H. *Acta Crystallogr.* **2010**, *D66*, 213−221.
(41) Winn, M. D.; Isupov, M. N.; Murshudov, G. N. *Acta Crystallogr.* **2001**, *D57*, 122−133.

DOI: 10.1021/jacs.5b01202
J. Am. Chem. Soc. 2015, 137, 5980−5989